The Journal of Chemical Physics

Does electronic coherence enhance anticorrelated pigment vibrations under realistic conditions?

Cite as: J. Chem. Phys. **151**, 114115 (2019); https://doi.org/10.1063/1.5119248
Submitted: 11 July 2019 . Accepted: 30 August 2019 . Published Online: 20 September 2019

Hong-Guang Duan, Michael Thorwart, and R. J. Dwayne Miller

COLLECTIONS

Paper published as part of the special topic on Ultrafast molecular sciences by femtosecond photons and electrons
Note: The paper is part of the JCP Special Topic on Ultrafast Molecular Sciences by Femtosecond Photons and Electrons.

View Online Export Citation CrossMark

ARTICLES YOU MAY BE INTERESTED IN

On the calculation of quantum mechanical electron transfer rates
The Journal of Chemical Physics **151**, 114119 (2019); https://doi.org/10.1063/1.5116800

X-ray linear and non-linear spectroscopy of the ESCA molecule
The Journal of Chemical Physics **151**, 114110 (2019); https://doi.org/10.1063/1.5116699

Ultrafast photoelectron spectroscopy of aqueous solutions
The Journal of Chemical Physics **151**, 090901 (2019); https://doi.org/10.1063/1.5098402

Challenge us.
What are your needs for periodic signal detection?
Zurich Instruments
Watch

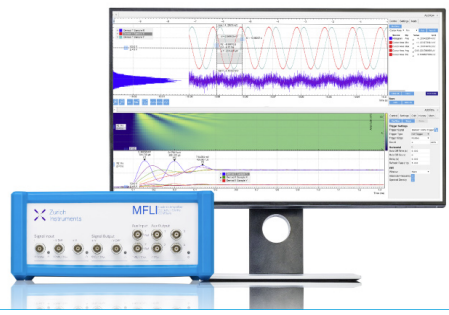

© 2019 Author(s).

The Journal of Chemical Physics ARTICLE scitation.org/journal/jcp

Does electronic coherence enhance anticorrelated pigment vibrations under realistic conditions?

Cite as: J. Chem. Phys. 151, 114115 (2019); doi: 10.1063/1.5119248
Submitted: 11 July 2019 • Accepted: 30 August 2019 •
Published Online: 20 September 2019

View Online Export Citation CrossMark

Hong-Guang Duan,[1,2,3] Michael Thorwart,[2,3,a)] and R. J. Dwayne Miller[1,3,4,b)]

AFFILIATIONS

[1] Max Planck Institute for the Structure and Dynamics of Matter, Luruper Chaussee 149, 22761 Hamburg, Germany
[2] I. Institut für Theoretische Physik, Universität Hamburg, Jungiusstraße 9, 20355 Hamburg, Germany
[3] The Hamburg Center for Ultrafast Imaging, Luruper Chaussee 149, 22761 Hamburg, Germany
[4] The Departments of Chemistry and Physics, University of Toronto, 80 St. George Street, Toronto, Ontario M5S 3H6, Canada

Note: The paper is part of the JCP Special Topic on Ultrafast Molecular Sciences by Femtosecond Photons and Electrons.
[a)] **Electronic mail:** michael.thorwart@physik.uni-hamburg.de
[b)] **Electronic mail:** dwayne.miller@mpsd.mpg.de

ABSTRACT

The light-harvesting efficiency of a photoactive molecular complex is largely determined by the properties of its electronic quantum states. Those, in turn, are influenced by molecular vibrational states of the nuclear degrees of freedom. Here, we reexamine two recently formulated concepts that a coherent vibronic coupling between molecular states would either extend the electronic coherence lifetime or enhance the amplitude of the anticorrelated vibrational mode at longer times. For this, we study a vibronically coupled dimer and calculate the nonlinear two-dimensional (2D) electronic spectra that directly reveal electronic coherence. The time scale of electronic coherence is initially extracted by measuring the antidiagonal bandwidth of the central peak in the 2D spectrum at zero waiting time. Based on the residual analysis, we identify small-amplitude long-lived oscillations in the cross-peaks, which, however, are solely due to groundstate vibrational coherence, regardless of having resonant or off-resonant conditions. Our studies neither show an enhancement of the electronic quantum coherence nor an enhancement of the anticorrelated vibrational mode by the vibronic coupling under ambient conditions.

Published under license by AIP Publishing. https://doi.org/10.1063/1.5119248

I. INTRODUCTION

In the initial steps of photosynthesis, photoactive molecular complexes capture the sunlight energy and transfer it to the reaction center on an ultrafast time scale with unity quantum efficiency.[1] The performance is determined by the molecular electronic properties, in concert with the molecular vibrations and coupling to the environment given by a solvent and the surrounding pigments and proteins. To investigate the energy transfer, ultrafast 2D electronic spectroscopy[2–4] is able to resolve femtosecond time scales. It is able to reveal the interactions between the energetically close-by lying molecular electronic states, for which the linear spectra are commonly highly congested and broadened by the strong static disorder.[5] Recent experimental studies of the Fenna-Matthews-Olson (FMO) complex reported long-lived oscillations of the cross-peaks both at low[6] and at room temperatures,[7] which have been assigned to enhanced electronic coherence. This has generated tremendous interest in this new field of quantum biology,[8] aiming to reveal a functional connection between photosynthetic energy transfer and long-lived quantum coherence. Moreover, also in photoactive marine cryptophyte algae,[9] the light-harvesting complex LHCII,[10] and the Photosystem II reaction center,[11,12] long-lived oscillations have been experimentally reported at low and room temperatures.

To model the reported[6] coherence, Ishizaki and Fleming have used a parametrized model of the FMO complex,[13] with a rather small reorganization energy of 35 cm^{-1} to fit the electronic coherence time scale.[14] This value was extracted[15] from fluorescence

Published under license by AIP Publishing

line narrowing measurements at low temperature[16] and does not include high-frequency intramolecular modes. However, even with the small reorganization energy, Shi *et al.* have calculated the complete 2D spectra and found a much shorter electronic coherence lifetime.[17] They have pointed out that the interpretation of the long-lived coherence could just be due to the intentional magnification of the 2D spectral amplitudes by the deliberately used inverse hyperbolic sine scale. In addition, electronic quantum coherence has been questioned to play any crucial role for the energy transfer as the transport is dominated largely by incoherent exciton relaxation.[18,19] A critical issue has been the use of an inadequate spectral distribution of the environmental fluctuations. The experimentally determined spectral density with a larger reorganization energy[15] has been used to calculate the dynamics by the quasiadiabatic propagator path integral.[18] There, a local vibrational mode at 180 cm^{-1} with a broadening of 29 cm^{-1} has been included with a total reorganization energy of 100 cm^{-1}. The numerically exact results also show a significantly shorter electronic coherence lifetime. Recent QM/MM-simulations[20–24] yield site-resolved spectral densities with reorganization energies of 150–200 cm^{-1}. Moreover, it has been shown in a dimer model that after a short decoherence time, the system relaxes to the polaron state due to strong electronic dephasing, which introduces static coherence in the exciton basis.[25] This static coherence (or spatial delocalization) of the excitons, which originates from the system-bath entanglement, is persistent and can be relevant for energy transfer.[18]

Thus, theoretical studies showed that pure electronic quantum coherence cannot survive under ambient conditions. Motivated by this disagreement, the coherent exciton dynamics in the FMO complex has been reexamined experimentally by 2D electronic spectroscopy.[26] A fit to an Ohmic spectral density with a broadened effective high-frequency mode yields a reorganization energy of 190 cm^{-1}. The observed lifetime of the electronic coherence of ~60 fs is too short to play any functional role in the energy transport, which occurs of the picosecond time scale.

In addition to the electronic coherence, signatures of the vibrational coherence of the pigment-protein host can also be accessed on the same spectroscopic footing.[27–30] Yet, electronic coherence can be distinguished from vibrational coherence.[31,34,35] Long-lived pure electronic coherence is unexpected to exist in most light-harvesting complexes. However, long-lived vibrational coherence is common and is not expected to strongly affect light-harvesting in the first place. Two concepts are currently under debate: (i) In 2013, Plenio *et al.*[32] argued that long-lived vibrationally coherent modes can significantly enhance the electronic coherence lifetime when the vibrational and electronic degrees of freedom are resonantly coupled. The vibrational mode is supposed to act as a "phonon laser" on the excitons, thereby producing ultralong electronic coherence. (ii) Moreover, Tiwari *et al.*[33] argued that nonadiabatic electronic-vibrational coherent mixing at short times resonantly enhances the amplitude of the particular delocalized anticorrelated vibrational mode in the ground electronic state. This second concept does not involve long-lived electronic coherence and is conceptually in agreement with the observation that a strong vibronic coupling produces large-amplitude coherent oscillations of the electronic component with a usual short lifetime and a long-lived vibrational coherence, but with a rather small amplitude.[34,35] This scenario was reexamined again recently[36] with an explicit coupling to an electronic and a vibrational bath. The result that an increased vibronic coupling survives weak electronic dephasing at short times and induces a resonantly enhanced long-lived vibrational coherence of the anticorrelated mode was presented as an explanation of the long-lived coherence signals observed in Ref. 6. However, again, an unrealistically weak electronic damping with a reorganization energy of 35 cm^{-1} has been used.

Motivated by this discrepancy, we have reexamined the coherent dynamics in a model of a vibronically coupled excitonic dimer with anticorrelated pigment vibrations being a minimal model to reveal the principal mechanism at work. We calculate the 2D electronic spectra of the model dimer with a typical energy gap as being part of the FMO complex. We use the environmental parameters obtained from the recent FMO experiment.[26] We examine the electronic coherence lifetime by the antidiagonal bandwidth of the diagonal peak at zero waiting time. The oscillations in the residuals obtained from the global fitting analysis confirm that the long-lived coherence is purely vibrational in nature, irrespective of resonant or nonresonant conditions. To distinguish the coherent dynamics of the electronic excited state, we have calculated the dynamics of the electronic wave packet on the vibrational potential energy surfaces (PESs), accompanied by the projection onto the reaction coordinates. Also here, the vibrational coherence is clearly identified by the oscillations close to the potential minimum. The projection shows that the long-lived oscillations are solely of vibrational origin, which confirms the 2D spectroscopic calculations. Moreover, we show that under realistically strong electronic damping, coherent vibronic coupling at short times does not enhance the amplitude of the anticorrelated vibrational mode, while we recover the mechanism of vibronic enhancement only for unrealistically weak electronic damping.

II. THEORY

The model is described by a total Hamiltonian consisting of the system, bath, and system-bath interaction terms, $H = H_S + H_{SB}$. The system is a dimer consisting of monomers A and B with site energies $E_{A/B}$, both having the same electronic ground state $|g\rangle$ and the respective electronic single excited states $|A\rangle$ and $|B\rangle$. The double excited state is denoted as $|AB\rangle$. Each electronic excited state couples to a vibrational mode (each to its own mode). The two couplings are such that an anticorrelated out-of-phase oscillation of the two electronic states occurs. In the exciton site basis, we have

$$H_S = |g\rangle h_g \langle g| + |A\rangle h_A \langle A| + |B\rangle h_B \langle B| + (|A\rangle V \langle B| + h.c.) + |AB\rangle (h_A + h_B) \langle AB|. \quad (1)$$

Here, $h_g = \frac{1}{2}\Omega(P^2_{A/B} + Q^2_{A/B})$, $h_A = E_A + h_g - \kappa Q_A$, and $h_B = E_B + h_g + \kappa Q_B$, respectively. $P_{A/B}$ and $Q_{A/B}$ are the momenta and the coordinates of the two vibrational modes coupled to monomers A and B. We express the vibronic coupling strength between the ground and excited states as $\kappa = \frac{\Omega\Delta}{\sqrt{2}}$, where Δ is the dimensionless shift of the excited state relative to its ground state. Ω is the vibrational frequency (both modes are taken with equal characteristics). V denotes the electronic coupling between two electronic excited states $|A\rangle$ and $|B\rangle$.

Published under license by AIP Publishing

For the discussion of the anticorrelated vibrations, it is useful to define new coordinates and momenta according to $Q_\pm = \frac{1}{\sqrt{2}}(Q_A \pm Q_B)$ and $P_\pm = \frac{1}{\sqrt{2}}(P_A \pm P_B)$.[37] Then, the system Hamiltonian can be written as

$$
\begin{aligned}
H_S &= \sum_{n=0,1,2} H_{S,n} = \sum_{n=0,1,2} (H^+_{S,n} + H^-_{S,n}),\\
H^-_{S,0} &= \mathbf{1}_0 h^-,\\
H^-_{S,1} &= \mathbf{1}_1 h^- + (E_B - \Omega Q_- \Delta/\sqrt{2})|B\rangle\langle B| + (E_A + \Omega Q_- \Delta/\sqrt{2})\\
&\quad \times |A\rangle\langle A| + V(|A\rangle\langle B| + |B\rangle\langle A|),\\
H^-_{S,2} &= \mathbf{1}_2 (h^- + E_A + E_B),
\end{aligned}
\tag{2}
$$

with $[H^+_{S,n}, H^-_{S,n}] = 0$ and $H^+_{S,n} = \mathbf{1}_n(h^+ - n\Omega Q_+ \Delta/\sqrt{2})$. The two rotated vibrational modes are given by $h^\pm = \frac{1}{2}\Omega(P^2_\pm + Q^2_\pm)$, and the projection operators are $\mathbf{1} = \sum_{n=0,1,2}\mathbf{1}_n$ with $\mathbf{1}_0 = |g\rangle\langle g|$, $\mathbf{1}_1 = |A\rangle\langle A| + |B\rangle\langle B|$, and $\mathbf{1}_2 = |AB\rangle\langle AB|$. The transformation of the Hamiltonian is illustrated in Fig. 1.

We choose the same parameters as in Ref. 33 for the system Hamiltonian. This dimer mimics one exciton pair of the FMO complex. The bath part will be discussed below (in particular, we do not choose the same parameters of too weak damping but use our own parameters of Ref. 26). The electronic energy gap is set to $E_A - E_B = 150\ \mathrm{cm}^{-1}$, and the electronic coupling is $V = 66\ \mathrm{cm}^{-1}$. Moreover, the dimensionless vibrational shift is set to $\Delta = 0.2236$. The pure electronic energy gap without coupling can then be calculated to be $\Delta E = 200\ \mathrm{cm}^{-1}$. As in Ref. 33, we model inhomogeneous broadening by a static Gaussian disorder of width $\delta E = 26\ \mathrm{cm}^{-1}$. For the vibrational mode, we choose the frequency $\Omega = 200\ \mathrm{cm}^{-1}$ that corresponds to the resonant case when the vibronic coupling vanishes (the slight shift of this resonance due to the vibronic coupling does not alter the overall result since we find essentially the same conclusion also for the off-resonant case; see below).

The environment and coupling part $H_{SB} = H^{\mathrm{vib}}_{SB} + H^{\mathrm{el}}_{SB}$ consist of two parts, the vibrational baths that damp the vibrational motions and the electronic bath that generates electronic dephasing and damping. In general, we assume Gaussian fluctuations described in terms of the standard model of dissipative quantum systems. The electronic environment is generated by fluctuating charges in the protein and the solvent and consists of two harmonic oscillator baths, each of which couples to the electronic excited states of monomers A and B, respectively. Thus, we have the Hamiltonian $H^{\mathrm{el}}_{SB} = \sum_{\alpha=A,B} H^{\mathrm{el}}_{SB,\alpha}$ with

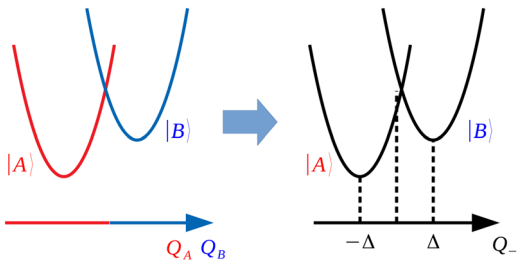

FIG. 1. The vibronic dimer model in Eq. (1) can be transformed into Eq. (2).

$$
H^{\mathrm{el}}_{SB,\alpha} = \frac{1}{2}\sum_{i=1}^{N}\left[\frac{p^2_{i,\alpha}}{m_{i,\alpha}} + m_{i,\alpha}\omega^2_{i,\alpha}\left(x_{i,\alpha} - \frac{c_{i,\alpha}|\alpha\rangle\langle\alpha|}{m_{i,\alpha}\omega^2_{i,\alpha}}\right)^2\right]. \tag{3}
$$

As usual, $p_{i,\alpha}$ and $x_{i,\alpha}$ are the momenta and the coordinates of the ith bath mode coupling to the electronic state $\alpha = A, B$. For the electronic part, we choose an Ohmic spectral density with the parameters obtained from fitting the linear spectra of the FMO complex to experimental data (see Ref. 26). Note that these values correspond to much stronger damping than those in Ref. 33. Thus, each bath is assumed to have its own but equal spectral density $J^{\mathrm{el}}(\omega) = \gamma^{\mathrm{el}}\omega\exp(-\omega/\omega_c)$ with $\gamma^{\mathrm{el}} = 0.7$, $\omega_c = 350\ \mathrm{cm}^{-1}$.

The vibrational environment roots in fluctuating nuclear degrees of freedom of the protein and couples to the vibrational displacements Q_A or Q_B of the mode coupled to the electronic state A or B. Hence, $H^{\mathrm{vib}}_{SB} = \sum_{\alpha=A,B} H^{\mathrm{vib}}_{SB,\alpha}$ with

$$
H^{\mathrm{vib}}_{SB,\alpha} = \frac{1}{2}\sum_{i=1}^{N}\left[\frac{q^2_{i,\alpha}}{\mu_{i,\alpha}} + \mu_{i,\alpha}\nu^2_{i,\alpha}\left(y_{i,\alpha} - \frac{d_{i,\alpha}Q_\alpha}{\mu_{i,\alpha}\nu^2_{i,\alpha}}\right)^2\right]. \tag{4}
$$

$q_{i,\alpha}$ and $y_{i,\alpha}$ are the momenta and the coordinate of the ith vibrational bath mode of the state $\alpha = A, B$. We assume that the vibrational bath has the same spectral density as the electronic bath, i.e., $J^{\mathrm{vib}}(\omega) = \gamma^{\mathrm{vib}}\omega\exp(-\omega/\omega_c)$, but with weaker damping, $\gamma^{\mathrm{vib}} = 0.02$ and $\omega_c = 350\ \mathrm{cm}^{-1}$.

To disentangle electronic and vibrational coherence, we perform a projection of the electronic wave packet on the reaction coordinate, which allows us to distinguish the vibrational coherence from the vibronic dynamics. We assume the initial wave packet to be in the lowest vibrational state $|0\rangle$ of the electronic excited state $|A\rangle$ in the site basis such that the initial density matrix can be written as $\rho(0) = |A, 0\rangle\langle A, 0|$. In order to obtain dynamical information, we determine the probability of the wave packet along the reaction coordinate Q_- by the time-dependent projection

$$
P^{ad}_{\tilde{k}}(Q_-, t) = \langle Q_-|\langle\tilde{k}|\rho(t)|\tilde{k}\rangle|Q_-\rangle, \tag{5}
$$

where $P^{ad}_{\tilde{k}}$ is the probability density of the reaction coordinate and $\tilde{k}$ indicates the electronic state of A or B in the exciton basis (for details of the projection, see Refs. 38 and 39).

III. RESULTS AND DISCUSSION

We assume[33] that two perpendicular transitions from the common ground state to the two excited states of monomers A and B are possible. Hence, the transition dipole moments are fixed to $\vec{\mu}_A = \mu_A \mathbf{e}_x$ and $\vec{\mu}_B = \mu_B \mathbf{e}_y$ with $\mu_A = \mu_B = 1$. Here, $\mathbf{e}_j$ is the unit vectors in the direction j. Temperature is set to 300 K, if not stated otherwise. We use the time nonlocal quantum master equation[40–43] with the equation-of-motion phase-matching approach.[44] Details are given in the supplementary material Appendix of Ref. 26.

We first consider the vibronic dimer with resonant vibrational coupling for which we obtain the 2D electronic spectrum shown in Fig. 2(a) (real part). At waiting time $T = 0$ fs, the inhomogeneous broadening can be clearly identified because the spectrum is stretched along the diagonal. It disappears within 50 fs (see the time dependent 2D electronic spectra in the supplementary material). The corresponding 2D spectrum of the purely electronic dimer without vibrational modes is shown in Fig. 2(b). From the

Published under license by AIP Publishing

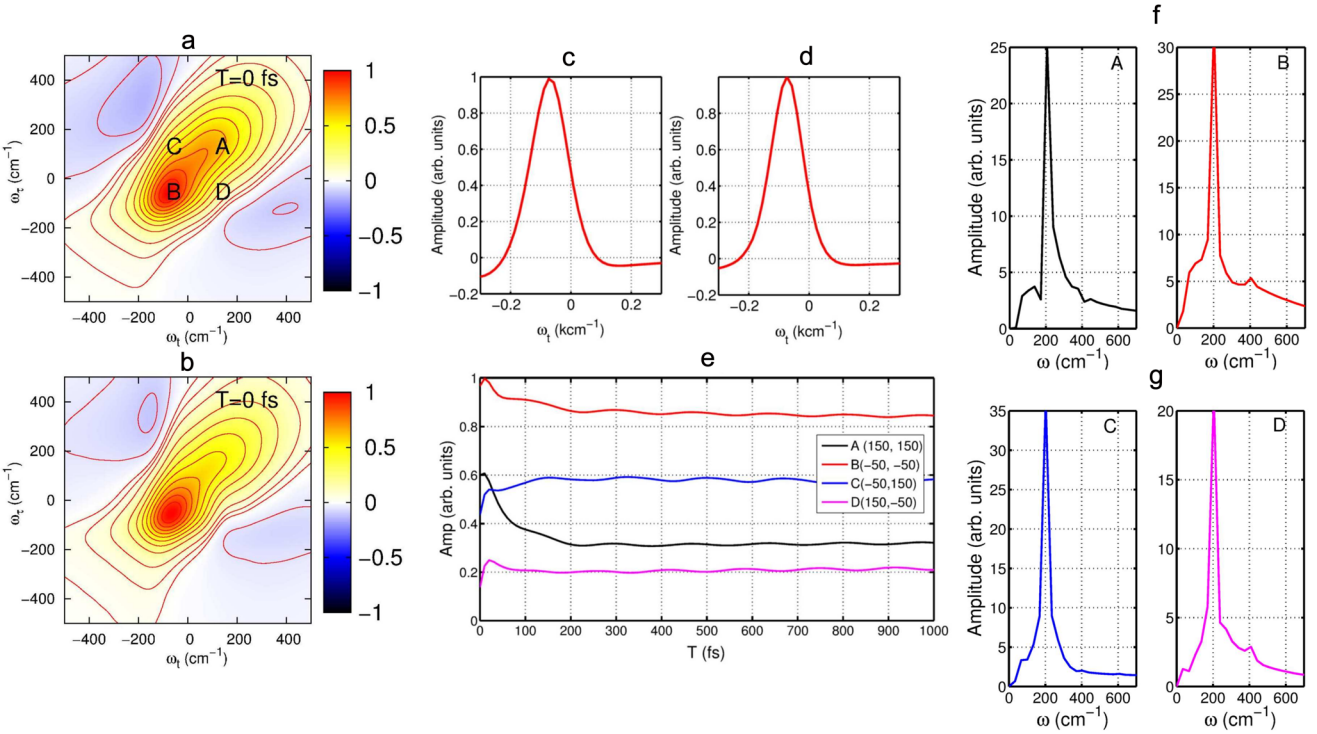

FIG. 2. (a) Real part of the 2D electronic spectrum of the vibronic dimer at room temperature (300 K). The diagonal peak A is located at (ω_t = 150 cm^{-1}, ω_τ = 150 cm^{-1}) and B at (ω_t = −50 cm^{-1}, ω_τ = −50 cm^{-1}). The off-diagonal peak C sits at (ω_t = −50 cm^{-1}, ω_τ = 150 cm^{-1}) and D at (ω_t = 150 cm^{-1}, ω_τ = −50 cm^{-1}). The time dependent trace of the selected peaks is shown in (e). For comparison, the 2D spectrum of the dimer without the effective vibrational mode is shown in (b). To obtain the time scale of the electronic dephasing, the antidiagonal profile of the peaks B in (a) and (b) are shown in (c) and (d). The resulting time scale of the electronic dephasing is 70 fs and 80 fs, respectively. [(f) and (g)] Power spectra of the peaks A, B, C, and D for the case with vibrational coupling. The broad background spectral band is associated with fast electronic dephasing. In addition to the strong vibrational peak at 200 cm^{-1}, one additional peak at 400 cm^{-1} is well resolved.

profiles taken along the antidiagonal band and shown in Figs. 2(c) and 2(d), we observe that the antidiagonal broadening of the 2D spectra in both cases is similar, which proves that both dimers undergo a similar dephasing dynamics with similar time scales of the electronic dephasing. They are extracted to be 70 fs and 80 fs, respectively. To resolve the time-dependent energy transfer, we analyze the series of 2D spectra for increasing waiting times by the global fitting approach (see the supplementary material for details). This yields the shortest lifetime of the decay associated spectra, which is induced by the peak broadening and by electronic dephasing. Both lifetimes coincide in both cases, which shows that a vibronic coupling does not alter the short-time electronic dephasing properties.

For a quantitative analysis of the dissipative dynamics in the presence of a vibrational coupling, we plot in Fig. 2(e) the time evolution of the magnitude of the peaks selected in Fig. 2(a). We observe that the dynamics can be clearly separated into two sectors: (i) fast electronic dephasing, which initially occurs on the time scale of ~70 fs, as already resolved by the analysis of the antidiagonal bandwidth and the global fitting approach. Moreover, (ii) long-lived oscillations with small amplitudes are resolved at longer times. In order to identify the origin of these long-lived oscillations, we perform a Fourier transform of the residual, which is obtained by subtracting the kinetics resolved by the global fitting. The result is shown in Figs. 2(f) and 2(g). The process of fast electronic dephasing is associated with the broad background spectral band with a maximum at 200 cm^{-1}. In addition, this broad band is overlapped by one sharp peak at the same frequency of 200 cm^{-1}. One additional narrow peak is resolved at 400 cm^{-1}. It originates from the vibrational coherence between the vibrational ground $|0\rangle$ and the second vibrational level $|2\rangle$ of the electronic ground state, i.e., it is of pure vibrational origin. This is further illustrated in Fig. S3 of the supplementary material, where the stick spectrum also indicates the clearly separated electronic and vibrational parts of which the eigenstates are composed. Hence, as a matter of fact, we can conclude that these narrow peaks at 200 cm^{-1} and 400 cm^{-1} only stem from the vibrational coherence of each monomer.

A. Off-resonance case

Up to here, we have studied the vibronic dimer for the resonant case $\Delta E = \Omega$. Next, we investigate the off-resonant case as well and choose Ω = 500 cm^{-1}. The results are shown in Fig. 3(a),

Published under license by AIP Publishing

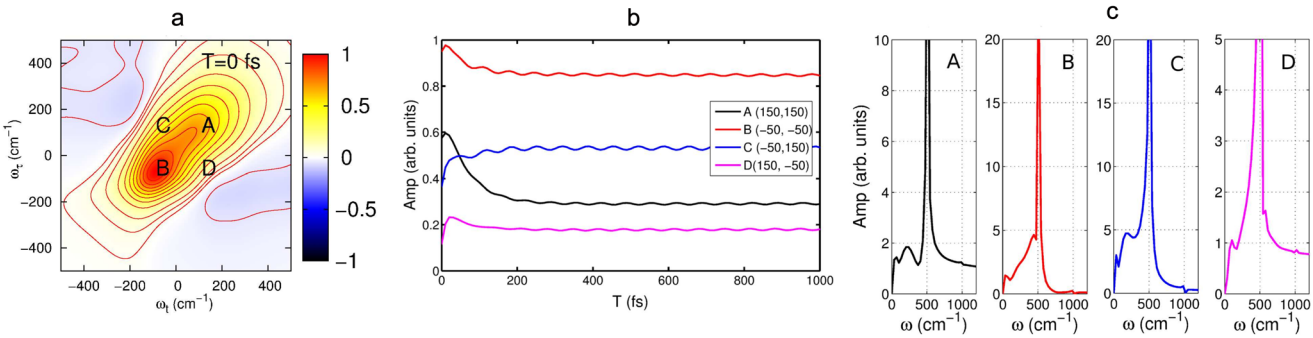

FIG. 3. (a) Real part of the 2D electronic spectrum of the vibronic dimer under off-resonant conditions with $\Omega = 500\ \text{cm}^{-1}$ at $T = 0$ fs. The kinetics of the selected peaks at A, B, C, and D are shown in (b), and the associated power spectra are shown in (c). To resolve the lifetime of the electronic coherence, we fit the broad peak at $200\ \text{cm}^{-1}$ with the Lorentzian lineshape and obtain the electronic coherence time of ~70 fs, which agrees with the resonant case.

and the global fitting analysis is shown in the supplementary material. The fast electronic dephasing with the time scale of 69 fs is still present. It agrees with the value of the antidiagonal bandwidth (see the supplementary material). Importantly enough, it coincides with the dephasing time scale of the resonant case. Hence, the fact that the electronic and vibrational dynamics are off-resonant does not affect the conclusion reached for the resonant case. In addition, we show in Fig. 3(b) the dynamics of the selected peaks for growing waiting times. It shows the same kinetics as in the resonant case: One fast electronic dephasing component is combined with a long-lived vibrational coherent component with a small amplitude. Again, we perform the Fourier transform of the residuals and plot the spectra of each peak in Fig. 3(c). We again find one broad band with a maximum at $200\ \text{cm}^{-1}$, which manifests the fast electronic dephasing and coincides with the lifetime of ~70 fs resolved by the global fitting approach. One clearly separated narrow peak is located at $500\ \text{cm}^{-1}$ with a large magnitude which is associated with the long-lived vibrational coherence. A clear evidence for the purely vibrational (and not vibronic) origin of the peak is that one additional peak can be resolved at $\sim 1000\ \text{cm}^{-1}$. It is the clear signature of the vibrational coherence between the vibrational ground $|0\rangle$ and the second vibrationally excited level $|2\rangle$ on the electronic ground-state surface.

B. Low-temperature case

Next, we consider the case of low temperature of 80 K. We follow the same steps as above and find for vanishing vibronic coupling $\kappa = 0$ an electronic dephasing time scale of 161 fs (see Fig. S4 in the supplementary material). In the presence of a resonant vibrational mode with $\Omega = 200\ \text{cm}^{-1}$ and with $\kappa \neq 0$ set to the same value as above, we obtain the dephasing time of 121 fs (see Fig. S3(b) in the supplementary material). It is slightly smaller than the one of the purely electronic case, but still comparable. The dynamics of the selected peaks in the 2D spectra again shows long-lived oscillations [see Fig. S3(c) of the supplementary material]. The Fourier transform, shown in Fig. S3(d), shows again one sharp peak at $200\ \text{cm}^{-1}$ and one additional peak at $400\ \text{cm}^{-1}$ with a quite weak magnitude. They manifest again the vibrational origin of the coherence. Therefore, we can conclude that, also for low temperature, the long-lived oscillation is just of vibrational origin. No different mechanism between low and room temperatures occurs.

C. Vibrational dynamics of the monomer

In addition to the dimer, we also investigate the monomer where only vibrational coherence is present. In Fig. S5(b) of the supplementary material, we show the time trace of the selected cross peak together with the Fourier spectrum in (c). The spectra are dominated by one peak at the vibrational frequency. An additional peak appears at the position of twice the vibrational frequency. Thus, the same scenario occurs for the monomer as well. We clearly demonstrate that the long-lived oscillations in a vibronically coupled dimer are just due to the overlap of the short-lived electronic coherence and the long-lived vibrational coherence.

D. Wave packet tracking

A further confirmation of this picture is obtained from monitoring the dynamics of the electronic excited states. For this, we project the time-evolved density matrix onto the anticorrelated vibrational coordinate Q_-. We use the same parameters as before and calculate the PESs of the electronic excited states $|\widetilde{A}\rangle$ and $|\widetilde{B}\rangle$ in the adiabatic basis. The result for the off-resonant case with $\Omega = 500\ \text{cm}^{-1}$ is shown in Figs. 4(a)–4(d). The initial wave packet is prepared in the excited state $|A\rangle$. For growing time, the transfer of population from $|\widetilde{A}\rangle$ to $|\widetilde{B}\rangle$ can be clearly identified by the decrease of the magnitude in Fig. 4(a) and the corresponding growth in Fig. 4(b). By this, the vibrational coherence of the excited states is clearly visible from the oscillations around the potential minimum [see Fig. 4(a)]. The oscillations have a period of ~66 fs, which exactly coincides with the assigned vibrational frequency of $500\ \text{cm}^{-1}$. Moreover, the population dynamics of the states $|\widetilde{A}\rangle$ and $|\widetilde{B}\rangle$ is shown in Fig. 4(c) by summing the wave packet population along the reaction coordinate Q_-. Spectral information can be again obtained from the Fourier transform. In Fig. 4(d), the vibrational coherence is identified by the narrow peaks at $500\ \text{cm}^{-1}$ and $1000\ \text{cm}^{-1}$,

Published under license by AIP Publishing

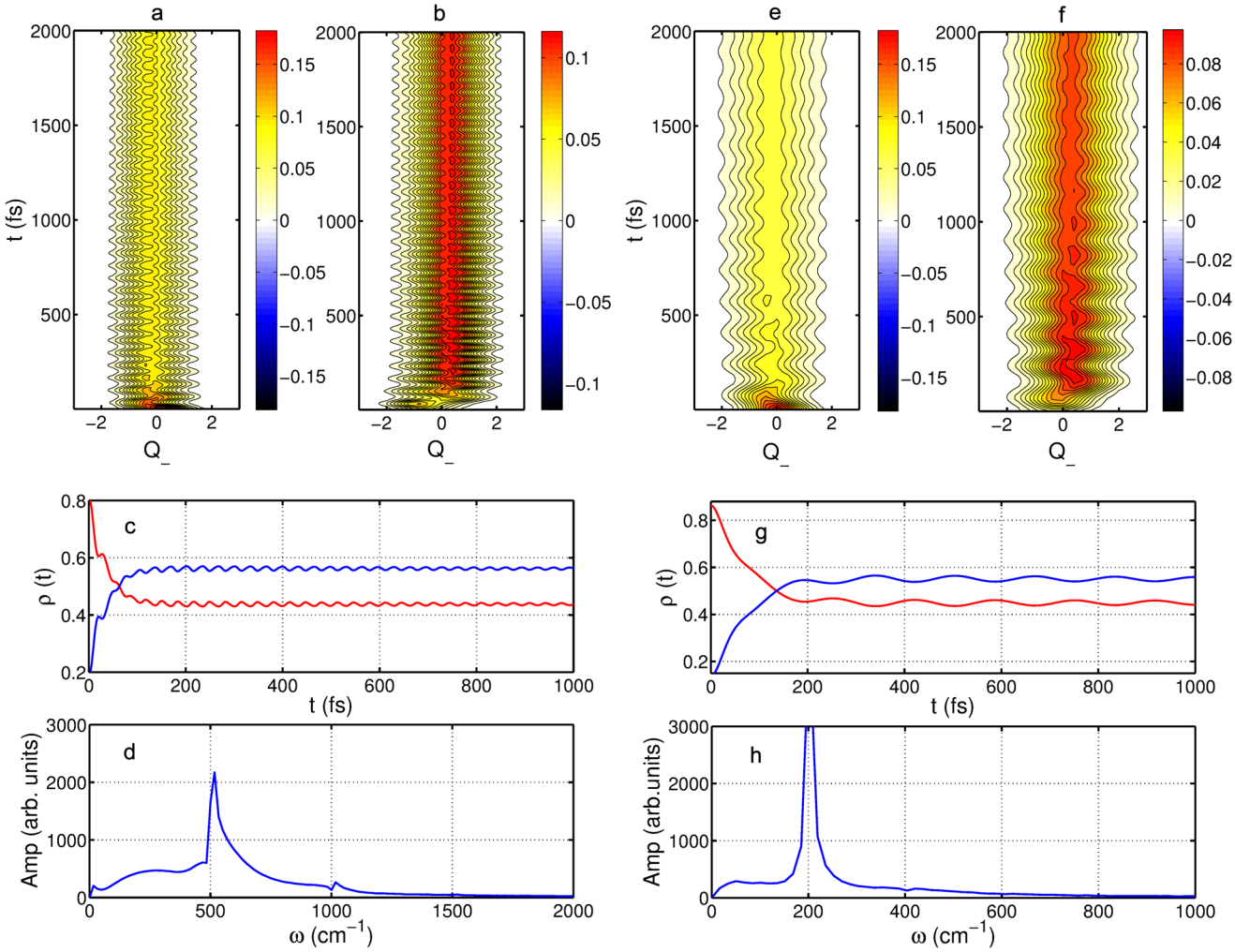

FIG. 4. Time evolution of the wave packet in the excited states $|\widetilde{A}\rangle$ (a) and $|\widetilde{B}\rangle$ (b). The integrated populations of the electronic states $|\widetilde{A}\rangle$ and $|\widetilde{B}\rangle$ obtained by summing along the reaction coordinate Q_- are shown in (c), together with the Fourier transform of the residuals in (d). The long-lived vibrational coherence is identified by the narrow peaks at 500 cm^{-1} and 1000 cm^{-1}. In addition, one broadband peak at 200 cm^{-1} represents the short-lived electronic coherence. The corresponding results of the resonant case are shown in (e)–(h), respectively. The long-lived vibrational coherence can be identified by the narrow peak at 200 cm^{-1} and the small dip at 400 cm^{-1}.

which coincide with the results from the 2D spectroscopic calculations shown in Fig. 3. In addition, a broadband background with a maximum at 200 cm^{-1} and with a small magnitude is visible, which again provides evidence of the electronic coherence being short-lived.

The resonant case, with $\Omega = 200$ cm^{-1}, is addressed in Figs. 4(e) and 4(f). Compared to the off-resonant case, no significant difference occurs. The initial wave packet in the excited state $|\widetilde{A}\rangle$ is transferred to $|\widetilde{B}\rangle$ over time. The only difference is the vibrational oscillation period of ~165 fs. The integrated time-dependent populations are shown in Fig. 4(g), and the associated spectral information is shown in Fig. 4(h). One narrow peak at 200 cm^{-1} and one additional dip at 400 cm^{-1} with quite small magnitude occur. Also here, the result agrees with the observation of the 2D spectroscopic calculations in Fig. 2.

E. Vibronic dimer under weak electronic dephasing

Up to here, we have studied the realistic parameters of the electronic dephasing and the vibrational damping constants. The possibility remains that for weaker electronic dephasing, the role of a coherent vibronic coupling could be more pronounced. This is not the case that follows from the dynamics of a vibronic dimer in the off-resonant case with $\Omega = 500$ cm^{-1} under (unrealistically) weak electronic dephasing. For this, we set $\gamma^{el} = \gamma^{vib} = 0.02$ and $\omega_c = 50$ cm^{-1}. The wave packet dynamics projected to the PESs

Published under license by AIP Publishing

of $|\widetilde{A}\rangle$ and $|\widetilde{B}\rangle$ is shown in Figs. 5(a) and 5(b), respectively. The purely vibrational coherence can be seen from the wave packet oscillations around $Q_- = -1.5$ with a period of ~67 fs, which coincides with the vibrational period. The electronic coherence is visible in Fig. 5 as a large-amplitude population exchange between the two electronic states. The electronic oscillation period of ~167 fs corresponds to the electronic energy gap $\Delta E = 200$ cm^{-1} in the adiabatic basis. Thus, the large-amplitude exchange is caused by the superposition of the wave packet components on the two PESs. To reveal the oscillation components and their lifetimes, we sum the wave packet components along the reaction coordinate and plot it in Fig. 5(c). The Fourier spectrum is shown in Fig. 5(d). Two large peaks at 200 cm^{-1} and 500 cm^{-1} correspond to the oscillations due to electronic and vibrational coherence, respectively. Two small vibronic peaks at 500 − 200 = 300 cm^{-1} and 500 + 200 = 700 cm^{-1} are due to the vibronic mixing. Most importantly, although the frequencies indeed mix and additional peaks are generated, the line widths of the peaks at 200 cm^{-1}, 300 cm^{-1}, 500 cm^{-1}, and 700 cm^{-1} are 35 cm^{-1}, 40 cm^{-1}, 20 cm^{-1}, and 45 cm^{-1}, respectively, and are thus all comparable. This proves that the lifetime of the electronic coherence is not affected by vibronic coupling to a vibrational mode.

F. Impact of coherent vibronic coupling on anticorrelated vibrations

Finally, we address the possibility that a strong coherent vibronic coupling could enhance the amplitude of the anticorrelated component of the vibrational dynamics.[33,36] The latter is given by the magnitude of the vibrational peak in the Fourier spectrum of the wave-packet dynamics, as, e.g., shown in Figs. 4(d), 4(h), and 5(d). In Fig. 6, we show the amplitude of the anticorrelated vibration for increasing vibronic coupling Δ for weak ($\gamma^{el} = 0.02$) and strong ($\gamma^{el} = 0.7$) electronic dephasing. For increasing Δ, the mixing of the anticorrelated vibration with the electronic parts becomes stronger. Indeed, for weak electronic dephasing, we find an increase in the anticorrelated vibrational amplitude, which confirms the picture of Refs. 33 and 36. However, for the more realistic case of stronger

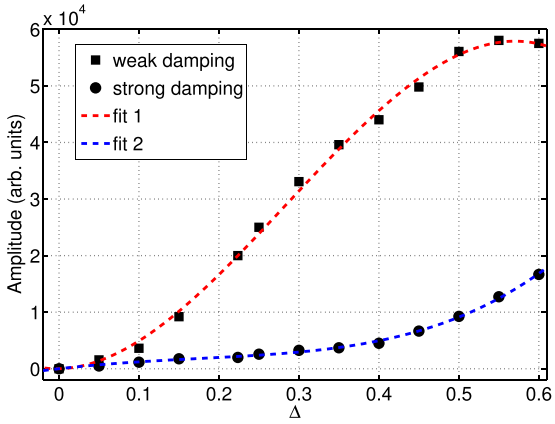

FIG. 6. Oscillation amplitude of the anticorrelated vibration vs the vibronic coupling strength Δ for weak ($\gamma^{el} = 0.02$, $\omega_c = 50$ cm^{-1}) and strong ($\gamma^{el} = 0.7$, $\omega_c = 350$ cm^{-1}) electronic dephasing for $\Delta E = 200$ cm^{-1}, $\Omega = 500$ cm^{-1}, and $T = 300$ K.

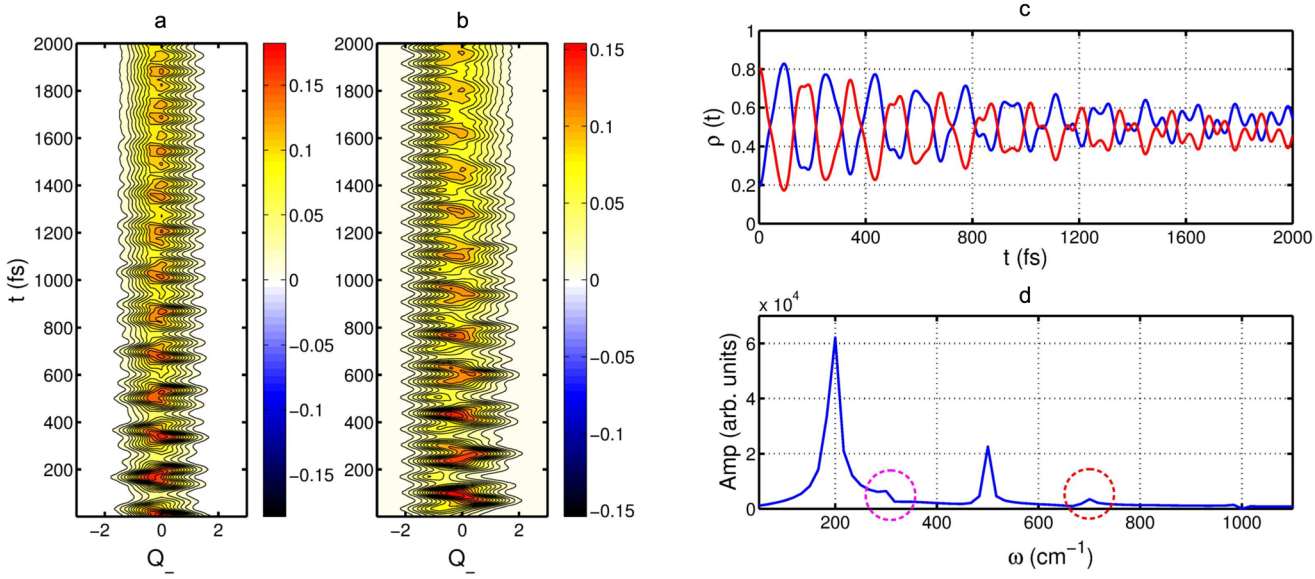

FIG. 5. Time evolution of the wave packet on the excited state PESs for $|\widetilde{A}\rangle$ is shown in (a) and for $|\widetilde{B}\rangle$ in (b) for the vibronic dimer under off-resonant conditions for very weak electronic dephasing $\gamma^{el} = \gamma^{vib} = 0.02$ and $\omega_c = 50$ cm^{-1}. The integrated populations of the electronic states $|\widetilde{A}\rangle$ and $|\widetilde{B}\rangle$ obtained by summing along the reaction coordinate Q_- are shown in (c), together with the Fourier transform of the residuals shown in (d). The vibronic coherence can be identified by the two peaks 300 cm^{-1} and 700 cm^{-1}, which are marked by circles.

Published under license by AIP Publishing

electronic dephasing, the amplitude of the anticorrelated vibration depends only weakly on the vibronic coupling since the coherent electron-vibrational mixing is dephased very rapidly and does not influence the vibration at later times.

IV. CONCLUSIONS

In conclusion, we have shown in a vibronic dimer model that, under typical ambient physical conditions, it is irrelevant for the lifetime of electronic quantum coherence in the excitation energy transfer whether the two exciton states couple to the two anticorrelated or correlated vibrational modes. This holds irrespective of whether the electronic and vibrational transitions are resonant or off-resonant and follows from an analysis of a model dimer in which each excited state is coupled to its own vibrational mode in an anticorrelated manner. Two independent baths for electronic dephasing as well as vibrational damping are included. By this, we clarify the question in the literature[32] whether a coupling to long-lived vibrational mode can lead to a substantial increase in the electronic coherence time. The conclusions are drawn from the calculated dynamics, the 2D electronic spectra, and the subsequent 2D global fitting approach. The exciton dynamics is characterized by the combination of a fast electronic dephasing and a long-lived vibrational coherent component, which has very small oscillation amplitudes. The long-lived oscillations are solely due to the coherence between different vibrational levels, irrespective of a resonant or an off-resonant vibronic anticorrelated coupling. Even under (unrealistically) weak electronic dephasing, the electronic coherence lifetime is not enhanced by the vibronic components. The same conclusion has been drawn from the study of indocarbocyanine dye molecules.[34] In addition, we find that a strong mixing of electronic and anticorrelated vibrational components of the wavefunction due to strong vibronic coupling does not enhance the vibrational amplitude at long times under ambient conditions. This effect can only occur under unrealistically weak electronic dephasing[33,36] but is unlikely to play a role in realistic physical systems, the reason being that the required coherent vibronic mixing is rapidly destroyed by fast electronic dephasing.

SUPPLEMENTARY MATERIAL

See the supplementary material for additional details on the time evolution of 2D electronic spectra of the vibronically coupled dimer, the global fitting approach, the decay associated spectrum and its form of the vibronically coupled dimer for both the resonant and off-resonant cases, and the comparison to the purely excitonic dimer model without vibrational coupling. Moreover, 2D electronic spectra for T = 77 K and of a monomer coupled to a vibrational mode are presented.

ACKNOWLEDGMENTS

We acknowledge financial support by the Max Planck Society and the Hamburg Centre for Ultrafast Imaging (CUI) within the German Excellence Initiative supported by the Deutsche Forschungsgemeinschaft.

REFERENCES

[1] R. E. Blankenship, "Antenna complexes and energy transfer processes," in *Molecular Mechanisms of Photosynthesis* (Blackwell Science, Oxford, Malden, 2002), pp. 61–94.
[2] D. M. Jonas, "Two-dimensional femtosecond spectroscopy," Annu. Rev. Phys. Chem. **54**, 425–463 (2003).
[3] M. L. Cowan, J. P. Ogilvie, and R. J. D. Miller, "Two-dimensional spectroscopy using diffractive optics based phased-locked photon echoes," Chem. Phys. Lett. **386**, 184–189 (2004).
[4] T. Brixner, T. Mančal, I. V. Stiopkin, and G. R. Fleming, "Phase-stabilized two-dimensional electronic spectroscopy," J. Chem. Phys. **121**, 4221–4236 (2004).
[5] S. Mukamel, "Nonlinear response functions and optical susceptibilities," in *Principles of Nonlinear Optical Spectroscopy* (Oxford University Press, Oxford, 1995), pp. 111–139.
[6] G. S. Engel *et al.*, "Evidence for wavelike energy transfer through quantum coherence in photosynthetic systems," Nature **446**, 782–786 (2007).
[7] G. Panitchayangkoona *et al.*, "Long-lived quantum coherence in photosynthetic complexes at physiological temperature," Proc. Natl. Acad. Soc. U. S. A. **107**, 12766–12770 (2010).
[8] N. Lambert, Y. N. Chen, Y. C. Cheng, C. M. Li, G. Y. Chen, and F. Nori, "Quantum biology," Nat. Phys. **9**, 10–18 (2013).
[9] E. Collini, C. Y. Wong, K. E. Wilk, P. M. G. Curmi, P. Brumer, and G. D. Scholes, "Coherently wired light-harvesting in photosynthetic marine algae at ambient temperature," Nature **463**, 644–647 (2010).
[10] G. S. Schlau-Cohen *et al.*, "Elucidation of the timescales and origins of quantum electronic coherence in LHCII," Nat. Chem. **4**, 389–395 (2012).
[11] F. D. Fuller, J. Pan, A. Gelzinis, V. Butkus, S. S. Senlik, D. E. Wilcox, C. F. Yocum, L. Valkunas, D. Abramavicius, and J. P. Ogilvie, "Vibronic coherence in oxygenic photosynthesis," Nat. Chem. **6**, 706–711 (2014).
[12] E. Romero, R. Augulis, V. I. Novoderezhkin, M. Ferretti, J. Thieme, D. Zigmantas, and R. van Grondelle, "Quantum coherence in photosynthesis for efficient solar-energy conversion," Nat. Phys. **10**, 676–682 (2014).
[13] A. Ishizaki and G. R. Fleming, "Theoretical examination of quantum coherence in a photosynthetic system at physiological temperature," Proc. Natl. Acad. Soc. U. S. A. **106**, 17255–17260 (2009).
[14] M. B. Plenio, J. Almeida, and S. F. Huelga, "Origin of long-lived oscillations in 2D-spectra of a quantum vibronic model: Electronic versus vibrational coherence," J. Chem. Phys. **139**, 235102 (2013).
[15] J. Adolphs and T. Renger, "How proteins trigger excitation energy transfer in the FMO complex of green sulfur bacteria," Biophys. J. **91**, 2778–2797 (2006).
[16] M. Wendling, T. Pullerits, M. A. Przyjalgowski, S. I. E. Vulto, T. J. Aartsma, R. van Grondelle, and H. van Amerongen, "Electron-vibrational coupling in the Fenna-Matthews-Olson complex of prosthecochloris aestuarii determined by temperature-dependent absorption and fluorescence line-narrowing measurements," J. Phys. Chem. B **104**, 5825–5831 (2000).
[17] L. Chen, R. Zheng, Y. Jing, and Q. Shi, "Simulation of the two-dimensional electronic spectra of the Fenna-Matthews-Olson complex using the hierarchical equations of motion method," J. Chem. Phys. **134**, 194508 (2011).
[18] P. Nalbach, D. Braun, and M. Thorwart, "Exciton transfer dynamics and quantumness of energy transfer in the Fenna-Matthews-Olson complex," Phys. Rev. E **84**, 041926 (2011).
[19] J. Wu, F. Liu, J. Ma, R. J. Silbey, and J. S. Cao, "Efficient energy transfer in light-harvesting systems: Quantum-classical comparison, flux network, and robustness analysis," J. Chem. Phys. **137**, 174111 (2012).
[20] M. K. Lee and D. F. Coker, "Modeling electronic-nuclear interactions for excitation energy transfer processes in light-harvesting complexes," J. Phys. Chem. Lett. **7**, 3171–3178 (2016).
[21] M. K. Lee, P. Huo, and D. F. Coker, "Semiclassical path integral dynamics: Photosynthetic energy transfer with realistic environment interactions," Annu. Rev. Phys. Chem. **67**, 639–668 (2016).
[22] S. A. Oh, D. F. Coker, and D. A. W. Hutchinson, "Optimization of energy transport in the Fenna-Matthews-Olson complex via site-varying pigment-protein interactions," J. Chem. Phys. **150**, 085102 (2019).

Published under license by AIP Publishing

[23]S. Chandrasekaran, M. Aghtar, S. Valleau, A. Aspuru-Guzik, and U. Kleinekathöfer, "Influence of force fields and quantum chemistry approach on spectral densities of BChl a in solution and in FMO proteins," J. Phys. Chem. B **119**, 9995–10004 (2015).
[24]C. Olbrich, J. Strümpfer, K. Schulten, and U. Kleinekathöfer, "Theory and simulation of the environmental effects on FMO electronic transitions," J. Phys. Chem. Lett. **2**, 1771–1776 (2011).
[25]J. Olšina, A. G. Dijkstra, C. Wang, and J. Cao, "Can natural sunlight induce coherent exciton dynamics?," e-print arXiv:1408.5385 (2014).
[26]H. G. Duan *et al.*, "Nature does not rely on long-lived electronic quantum coherence for photosynthetic energy transfer," Proc. Natl. Acad. Soc. U. S. A. **114**, 8493–8498 (2017).
[27]D. Egorova, "Self-analysis of coherent oscillations in time-resolved optical signals," J. Phys. Chem. A **118**, 10259–10267 (2014).
[28]V. Butkus *et al.*, "Vibrational vs. electronic coherences in 2D spectrum of molecular systems," Chem. Phys. Lett. **545**, 40–43 (2012).
[29]J. Seibt and T. Pullerits, "Beating signals in 2D spectroscopy: Electronic or nuclear coherences? Application to a quantum dot model system," J. Phys. Chem. C **117**, 18728–18737 (2013).
[30]C. Kreisbeck and T. Kramer, "Long-lived electronic coherence in dissipative exciton dynamics of light-harvesting complexes," J. Phys. Chem. Lett. **3**, 2828–2833 (2012).
[31]C. Kreisbeck, T. Kramer, and A. Aspuru-Guzik, "Disentangling electronic and vibronic coherences in two-dimensional echo spectra," J. Phys. Chem. B **117**, 9380–9385 (2013).
[32]A. W. Chin *et al.*, "The role of non-equilibrium vibrational structures in electronic coherence and recoherence in pigment–protein complexes," Nat. Phys. **9**, 113–118 (2013).
[33]V. Tiwari, W. K. Peters, and D. M. Jonas, "Electronic resonance with anti-correlated pigment vibrations drives photosynthetic energy transfer outside the adiabatic framework," Proc. Natl. Acad. Soc. U. S. A. **110**, 1203–1208 (2013).
[34]H. G. Duan *et al.*, "On the origin of oscillations in two-dimensional spectra of excitonically-coupled molecular systems," New J. Phys. **17**, 072002 (2015).
[35]A. Halpin *et al.*, "Two-dimensional spectroscopy of a molecular dimer unveils the effects of vibronic coupling on exciton coherences," Nat. Chem. **6**, 196–201 (2014).
[36]S.-H. Yeh, R. D. Hoehn, M. A. Allodi, G. S. Engel, and S. Kais, "Elucidation of near-resonance vibronic coherence lifetimes by nonadiabatic electronic-vibrational state character mixing," Proc. Natl. Acad. Soc. U. S. A. **116**, 18263 (2019).
[37]M. F. Gelin *et al.*, "Bath-induced correlations and relaxation of vibronic dimers," J. Chem. Phys. **136**, 034507 (2012).
[38]U. Manthe and H. Köppel, "Dynamics on potential energy surfaces with a conical intersection: Adiabatic, intermediate, and diabatic behavior," J. Chem. Phys. **93**, 1658–1669 (1990).
[39]D. Qi, H. G. Duan, Z. L. Sun, R. J. D. Miller, and M. Thorwart, "Tracking an electronic wave packet in the vicinity of a conical intersection," J. Chem. Phys. **147**, 074101 (2017).
[40]J. S. Cao, "A phase-space study of Bloch–Redfield theory," J. Chem. Phys. **107**, 3204–3209 (1997).
[41]C. Meier and D. J. Tannor, "Non-Markovian evolution of the density operator in the presence of strong laser fields," J. Chem. Phys. **111**, 3365–3376 (1999).
[42]U. Kleinekathöfer, "Non-Markovian theories based on a decomposition of the spectral density," J. Chem. Phys. **121**, 2505–2514 (2004).
[43]Y. C. Cheng and G. R. Fleming, "Coherence quantum beats in two-dimensional electronic spectroscopy," J. Phys. Chem. A **112**, 4254–4260 (2008).
[44]M. F. Gelin, D. Egorova, and W. Domcke, "Efficient method for the calculation of time- and frequency-resolved four-wave mixing signals and its application to photon-echo spectroscopy," J. Chem. Phys. **123**, 164112 (2005).

Published under license by AIP Publishing